Computing crustal deformation of the Iberian Peninsula

Author: Magí Romanyà Serrasolsas[1]
Advisor: Giorgi Khazaradze[2]
1. *Facultat de Física, Universitat de Barcelona, Diagonal 645, 08028 Barcelona, Spain*.*
2. *Facultat de Ciències de la Terra, Universitat de Barcelona, Martí i Franquès s/n, 08028 Barcelona, Spain*

Abstract: Crustal deformation studies are useful to comprehend on-going geological processes and enhance seismic hazard assessment studies. These studies require large GPS data sets, covering a wide temporal and spatial range, besides further complex computation and analysis. We present a three-dimensional crustal deformation velocity map of the Iberian Peninsula with improved spatial resolution. The results show a regional clockwise rotation of the peninsula, as well as a northward velocity trend in the eastern Betics. An explanation could involve a rigidly rotating lithospheric block along with a viscous coupling between Nubia and Eurasia plates. The results are coherent with earlier studies and will serve as a basis for future research.

I. INTRODUCTION

In this study we present a three-dimensional crustal deformation velocity field based on the analysis of data from ~400 continuous GPS antennas, scattered across the Iberian Peninsula and its surroundings regions covering a time-period of 11 years, starting in 2009 until 2021. Previous studies have already measured deformation in Iberia in 2015 [1], however, we present an improved spatial resolution and a vertical velocity field not measured before.

A. Crustal deformation

In physics, deformation refers to any change in shape, position or orientation of a body resulting from the application of stress. Crustal deformation is the deformation suffered by the earth's surface, induced by stress related to the moving tectonic plates. This deformation can be continuous, gradually changing the surface in secular motion or it can be sudden, generating earthquakes [2].

As said, tectonic plate motion explains the stress which cause crustal deformation. Plate tectonic theory postulates that earth's surface is broken up into tectonic plates which move with respect of one another. The plates are assumed to be spherical caps, with no internal deformations, which rotate at a constant rate about a Euler vector [2]. There are several models of plate motion, with different number and/or type of plates, made to fit different data and incorporate new observed phenomena.

Earthquakes can be explained by elastic rebound theory, which assumes that the crust can be modelled as an elastic material which can store stress. The build-up stress would be released suddenly causing an earthquake. This view also introduces the seismic cycle, which describes how the stress is being stored in large periods of time (~10-10 000 yr.) and then released abruptly during an earthquake. The large duration of the cycle makes it impossible to gather data of a fully completed one. Instead, it is common to work with multiple datasets of regions going through different stages of the cycle. Studies in crustal deformation and stress can be useful to predict natural disasters, forecasting risks and estimating where and when to expect one.

B. Seismotectonic setting

The Iberian Peninsula is characterized by the collision of the Nubia (Africa) and Eurasia plates during the last 120 Ma, which converge at rates of ~5 mm/yr [3]. This motion caused Iberia to undergo through a long process, first merging with the Eurasian plate, creating the Pyrenees mountain range around 30 Ma ago [4]. The Betics cordillera was also formed by the compression caused by the collision of the two plates.

The seismicity levels in the study area are between low and moderate, mainly concentrated in the Pyrenees and Betic mountain ranges (Fig. 1). The earthquakes in the south of the peninsula do not distribute in a line, instead they are scattered over a great area, indicating a diffuse boundary between the Africa and Eurasia plates. For the instrumentally measured earthquakes since 1910, only 3 have a M>7: 1954 Dúrcal, Granada, an event of magnitude 7.8 which occurred at 657 km depth. The other two events happened outside the peninsula, at Cabo de Sant Vicente in 1969 and at Asnam in 1980 with magnitudes of 7.8 and 7.3, respectively. The more devastating earthquakes in the peninsula happened before the start of instrumental measurements in 1910. Historical records account for at least 27 great earthquakes since the 14th century. The most significant ones include: a famously destructive 1755 Lisbon earthquake felt throughout Europe and causing a widespread tsunami and a high number of casualties; 1428 Queralbs earthquake in Catalonia [5]; 1829 Torrevieja in Valencia; and 1848 Arenas del Rey event in Andalusia [6].

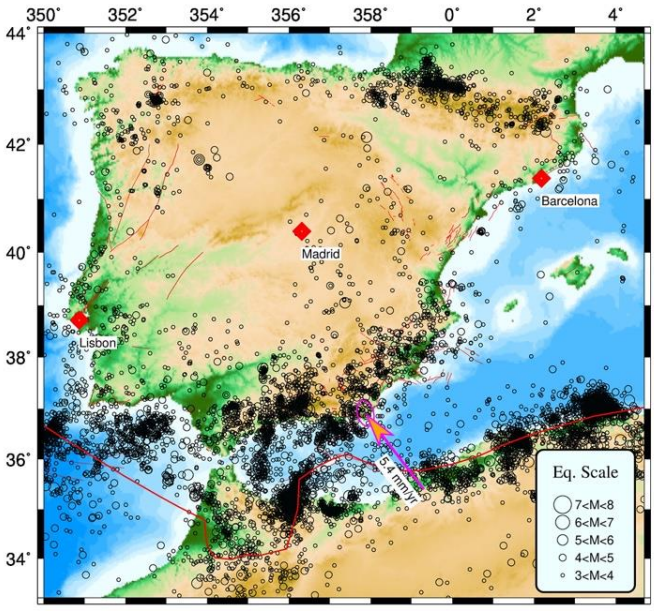

FIG. 1: Earthquake distribution in the Iberian Peninsula from 1910 to May 2022. The map shows the earthquakes as circles of different radius (see legend), red line shows Eurasia/Nubia plate boundary [7], and the relative motion between them with a pink vector [3]. The faults are displayed as orange lines [8].

* Electronic address: magiromanya@gmail.com

Due to the slow deformation in Iberia, a great accuracy is needed to be able to detect displacements rates of a few millimetres. To achieve such accuracy, GPS measuring techniques, alongside with further data analysis are required. GPS measurements, however, are relatively new, with the first 24-satellite GPS network first realized July 1992 [9]. Earthquakes before instrumental measurements were recorded from historical records or from paleoseismology.

II. METHODOLOGY

A. GPS System

Global Navigation Satellite System (GNSS) has become the standard way to measure geophysical phenomena in the last decades. In this work GPS signals are used. The Global Positioning System (GPS) is one of the global navigation satellite systems and is owned by the United States government. Unlike previous techniques, GPS provides three-dimensional positional coordinates with a high degree of accuracy. This data allows to measure vertical and horizontal displacements at the same time and position which results in more solid datasets. The inexpensive and precise nature of GPS, as well as its accessibility, makes it the perfect tool for research groups and universities.

In order to use GPS techniques to measure geological displacements, a great precision is needed, for we intend to measure distances in the order of millimetres. As it is presented in the results, in the Iberian Peninsula, the deformation varies from less than a millimetre a year to <5 mm/yr. However, raw GPS data can have big uncertainties, adding up to a few metres, making it unusable. It is crucial to understand the sources of error in GPS measurements to significantly lower the uncertainty and make them a viable option for geodetic surveys. In this section we will discuss how GPS technology works, study its sources of error, and how, if possible, decrease the uncertainties of our measurements.

Ideally, to determine a point in 3D space, a GNSS receiver would need 3 satellites. Using trilateration, by knowing the distance of the receiver to each satellite, it is possible to know where the receiver is in space. However, a fourth satellite is needed because it is crucial to synchronize the clocks of the satellites and the receivers as we will later discuss.

The main challenge in GPS technology is to accurately measure ranges, the distance between the receiver and the satellite. Ranges are calculated from time differences between the receivers and the satellites. As the signals propagate at the speed of light, which is very great (c = 299 792 458 m/s), GPS satellites carry highly precise atomic clocks on board to minimize the uncertainties.

A GPS satellite broadcasts radio signals in the so-called L-band part of the spectrum. It emits two carrier signals L1 (1575.42 MHz) and L2 (1227.60 MHz) [10], which are modulated to transmit codes of pseudorandom noise which carry information.

The pseudorange observable ($\mathrm{P_r^s}$), is the time difference between the receiver (T_r) and the satellite (T^s) multiplied by the speed of light.

$$P_r^s = c(T_r - T^s)$$

To compute this time difference, the receiver has a replica of the codes transmitted by the satellite and knows how far behind the signal is from its own. To deduce the range ρ_r^s from the pseudorange P_r^s, we must know the different errors there may be and how they affect the measurement. First, we must consider that the satellite and the receiver will not be synchronized, thus introducing a new unknown, clock bias defined as $\tau = T - t$ (difference between measured and true time). Second, we know that the radio signals do not always travel at the speed of light. The ionosphere and the troposphere can introduce delays ($\Delta I, \Delta T$) to the signal caused by refraction, which can change the speed and the direction of the signal. The following formula relates the pseudorange and the range assuming we know how each error contributes [10].

$$P_r^s(t) = \rho_r^s + c(\tau_r - \tau^s) + \Delta I + \Delta T + \epsilon$$

An additional term ϵ is added to represent other sources of error which include electrical noise from the receiver, signal scattering (multipath) and unmodeled motions of the satellites and station. The phase observable uses the L1 and L2 carrier waves to estimate the range. As the L1 and L2 signals are of lower wavelengths, the precision of the measurements is higher, and can be used for high precision applications as it is ours. In a similar fashion as the pseudorange observable, we can know the phase difference between the received signal and the replica of the receiver. This phase difference, however, skips an integer number of cycles N, which is unknown. A similar equation can be written for phase observable, adding the so-called integer ambiguity [10].

$$\phi_r^s(t) = \rho_r^s + c(\tau_r - \tau^s) + \lambda N - \Delta I + \Delta T + \epsilon$$

It is possible to take advantage of having two different channels L1 and L2 to mitigate the effect of the ionosphere, as the medium does affect differently two different wavelengths. A simple lineal combination of L1 and L2 creates a new frequency called LC or ionospheric-free signal defined as [10]:

$$\phi_{LC} = 2.546\phi_{L1} - 1.984\phi_{L2}$$

Clock bias is a combination of the bias in the satellite and in the receiver and can be countered by a technique called differencing. Between receivers differencing can eliminate the satellite bias by having two receivers listening to the same satellite. The satellite's clock will be off by the same amount in both receivers, making it possible to compute its value. In a similar manner, between satellites differencing makes the receiver's time bias banish, by making the receiver listen to two different satellites. This last difference is the reason why GPS needs 4 visible satellites for each receiver, three to solve for position and one for time. Using the two differencing techniques is called double differencing, and it is used in all GPS software to virtually eliminate time bias.

The LC frequency and differencing help to reduce certain errors; however, it is important to consider that using these techniques, which involve linear combinations of different signals, inevitably leads to the adding up of the errors from other sources (ϵ), present in the signal.

In this study, we have used both phase and pseudorange differencing, as well as the ionospheric-free signal LC with the software GAMIT.

B. GAMIT/GLOBK

GAMIT/GLOBK is a software developed at MIT made to analyse GNSS measurements specifically designed to study crustal deformation [10]. GAMIT stands for **G**NSS **a**t **MIT**. It is a collection of programs for processing phase data to accurately obtain relative positions of ground receivers. The software is capable of handling raw GPS data, and it has implemented algorithms to maximize the quality of the output via several techniques, some already discussed (differencing). GAMIT also handles pre-processing of the RINEX raw GPS files, generates the reference orbit and rotations of the satellites and must solve for the mentioned integer ambiguity in phase measurements, which is a complicated and computationally heavy task. GAMIT takes advantage of having information about multiple receivers to increase the accuracy of the results and can handle up to a maximum of 99 sites. However, the program computation complexity rises proportionally to the cube of the number of parameters, making working with more than 50 stations at a time impractical.

The output of GAMIT are h-files, which contain the processed data of the receivers as well as the estimated uncertainty of the values of a given day. The data inside h-files, are loose estimates of coordinates, called quasi-observations, meaning that they lack a reference frame. GLOBK is a set of tools developed at MIT, made to combine various geodesic solutions. It can combine quasi-observations "h-files" and to impose a reference frame, generating the final coordinates. In this work, the positions and velocities are in the ITRF2014 Eurasian plate reference frame [11], introduced using a GLOBK's tool called glred. In glred, the reference frame is introduced by assigning a priori knowledge of position and velocity of core stations fixed in our reference frame.

III. DATA

There are two main techniques to make GPS measurements: continuous or permanent (cGPS) and campaign or survey (sGPS) style observations. Specifically, most of the processed data came from cGPS (417) and the rest from sGPS (31). cGPS stations consist of permanent antennas fixed to one location. Unfortunately, less then 50 of them use specifically designed stable geodetic monuments. This type stations record data automatically and continuously, transferring it daily to the corresponding server, where the data is stored and distributed. Furthermore, cGPS has the advantage that observation time can be extensive, making the obtained measurements more precise. The long-term stability of GPS allows cGPS stations to be collecting data for years with minimal maintenance, outputting a continuous flow of data. In survey mode GPS (sGPS), specifically established geodetic monuments are measured using portable instruments (Fig. 2B) during the 2–3-day long campaigns, organized every 3-4 years. The output of this technique is a discrete dataset with 2-3 daily measurements seperated by several years (Fig. 4b). It is used to study coseismic and postseismic motions and to distinguish locked faults from creeping ones [2]. sGPS measurements are bound to be less precise due to errors in placing the antenna in the same place every campaign. Furthermore, the shorter observing sessions relative to cGPS can also damage the precision, as processing the data does not contribute much to lowering errors if there are few points to do statistics with.

FIG. 2: Example of geodetic monuments used in the study located at Cabo de Gata (Almeria). **A:** cGPS permanent station; **B:** sGPS monument with an antenna at RELL of the CuaTeNeo network [12].

GPS raw data is stored in RINEX files which can later be analysed by GAMIT. As we have described, continuous GPS outputs a constant stream of data. The data is transferred in a semiautomatic manner from the stations to data collecting servers which later can be accessed by scientists using the ftp protocol. Getting the data from the stations to the researcher's computer is outside of the scope of this work and can be found here.

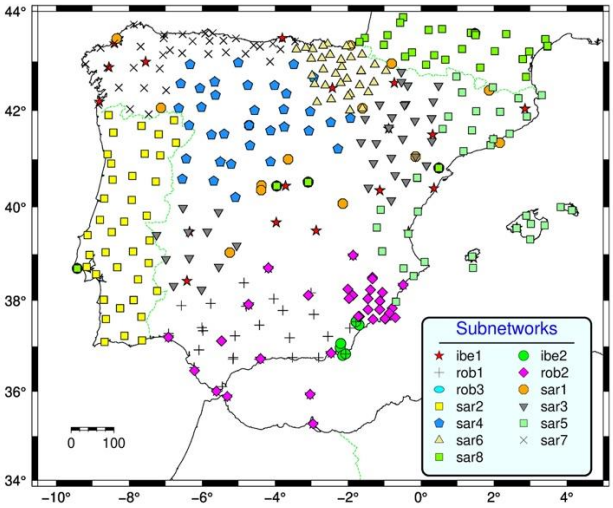

FIG. 3: Map with all the processed data and subnetworks. The map shows all the stations used in this TFG-thesis. The combination of colour and shape indicates the subnetwork in which they are.

As we have discussed in the methodology, GAMIT is optimized to process up 50 stations to compute the daily h-files. As in this study we have 417 stations, we must group the different stations in subnetworks, to be processed independently. These stations are plotted in Fig. 3, where it is easy to see the distribution of the subnetworks and their names. The subnetworks cannot be made up using random stations, it is important for the analysis that the stations are close together in a cluster. The subnetworks approach will output independent results that must be joined together to get a coherent picture of the peninsula's deformation. This is a difficult task, and it is done at the same time as introducing our reference frame. Glred has a suite of tools designed to join various geodetic solutions. Different subnetworks are combined and transformed into Eurasia fixed reference frames using common 13 core stations from Europe, used in each subnetwork.

IV. RESULTS

A. Time-series

Time series are the set of all the position coordinates, along with their uncertainties, of a single receiver over a certain period, which extends since the first measurements of said station. They are the result of all the data processing discussed in previous sections. Still, to interpret the results, further analysis is needed.

Multiple problems may affect the GPS antenna, causing anomalies which end up in the time-series data. There exists a variety of software to handle error analysis in time series, which tackles different problems. Offsets are a discontinuity in the data introduced by technical problems in the antenna, hardware or caused by an earthquake. It is easy to correct offsets via software, although it is important to mark where the offset happened, as the data around it is less reliable. Often, the cGPS stations stop functioning, creating a gap in the time series until the antenna is back online. In these situations, it is common for the data to contain an offset as well. In the time series we can expect outliers, points which are obviously not coherent with the rest, which must be removed.

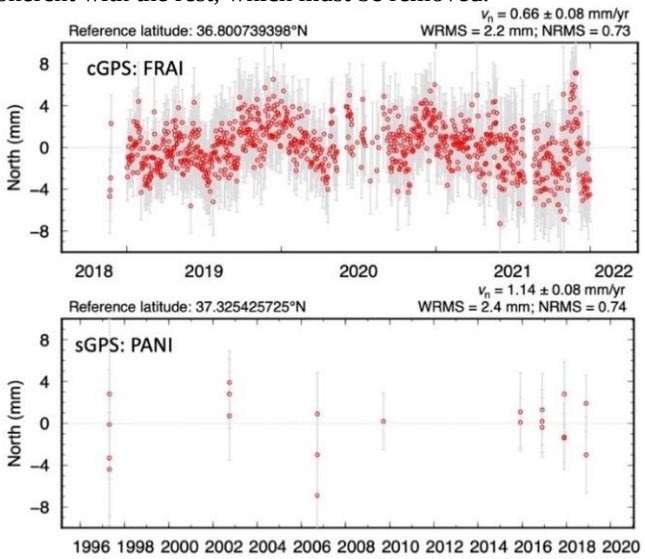

FIG. 4: GPS time series examples. **A:** Continuous GPS station FRAI near Cabo de Gata; **B:** Survey GPS station PANI located at Cala Panizo, Almería.

Provided that no earthquake happened, we would expect crustal deformation to be constant. Nonetheless, studying time-series results, one can detect oscillations which are not explained by crustal deformation. Software like *tsfit* and *tsview* [13], divides these oscillations in two terms: an annual term and a semi-annual term, as two sinusoidal waves [14]:

$$x^i = x_0^i + v_0^i(t - t_0) + A_0^i \cos\left(\frac{2\pi(t - t_0)}{T_0} - \tau_0\right) + \mathrm{A}_1^{\mathrm{i}} \cos\left(\frac{2\pi(t - t_0)}{T_1} - \tau_1\right)$$

The program can straighten the time-series, eliminating the identified oscillations, resulting in linear motion.

The coordinates come with their uncertainties which can be modelled as noise. The noise can be time independent "white noise" or time correlated "coloured noise". The modelling of the noise surrounding the data will be important later when we calculate the velocity field form the time-series.

B. Velocities

The three-dimensional velocity field is the final result of this work. The velocities are separated in two components: the horizontal (Fig. 5) and the vertical (Fig. 6) velocity fields.

From the time series, it is possible to estimate the velocity of the receiver, which is the rate of deformation of the site the antenna is located. The velocity field is a 3D vector map, where vertical deformation rates, due to the satellite geometry, have at least twice as big uncertainties. Horizontal velocity refers to the vector components tangent to the surface of earth. The horizontal velocity estimates are shown in Fig 5.

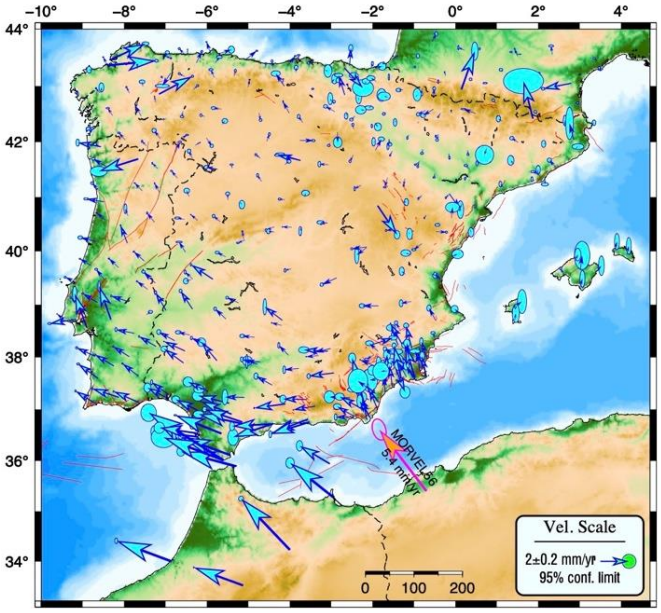

FIG. 5: Map of the horizontal velocities of the Iberian Peninsula. Uncertainty confidence limits are given at 95% level. The relative motion of Eurasia and Nubia is shown as a pink vector.

Differential motions between tectonic plates induce deformation along their boundaries [4]. This can be clearly seen in Fig. 5, where the larger deformation in the peninsula is in the south, nearest to the plate boundary, with motions around 4 and 5 mm/yr. The few stations in Africa also present high velocities (>5 mm/yr), which is what we would expect, as we are measuring in the Eurasian reference frame, and Africa is moving respect to it. In Iberia's centre there is a general lack of motion, as it is a stable zone showing no significant motion with respect to Eurasia reference frame. In the Pyrenees mountain range, no significant deformation is observed aside from a few outliers result of anomalies in the stations.

In the eastern region of the Betics, a consistent NNW decreasing velocity trend can be easily identified, which translates into a compression. This type of deformation could be explained by the transference of convergence rate of Nubia to this region by an independent tectonic block trapped between the Iberian-Nubia collision [1].

A regional clockwise rotation can be perceived in the western part of the peninsula, a result which was first identified in an earlier study [1], where the authors suggested that this rotation could be a result of shallow geodynamic process. However, they found limitations to this hypothesis, as there is

no evidence for significant seismicity or shear in the Iberian northern and easters margins. Alternatively, it was also suggested that the deeper geodynamic processes, involving viscous coupling of Nubia and Eurasia plates near the Gulf of Cádiz, are causing the observed rotation.

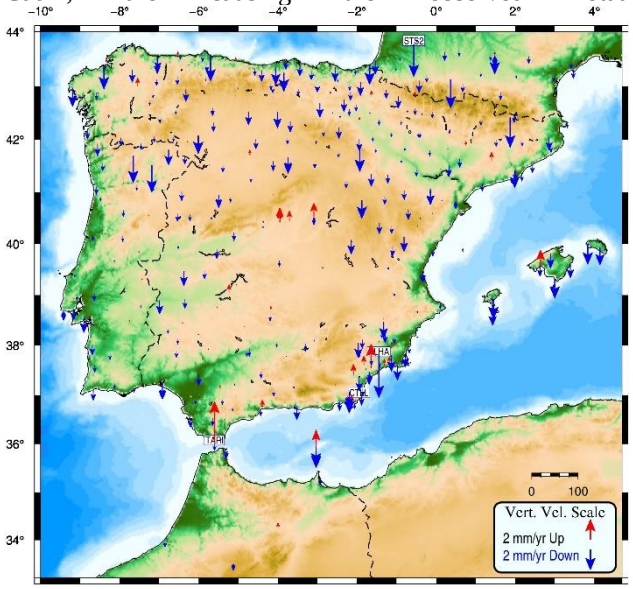

FIG. 6: Vertical velocity field from GPS measurements. The stations with a speed <5 mm/yr are excluded.

The vertical velocity field shown in Fig. 6, unlike the horizontal field, shows no obvious pattern. Although, the dominance of subsidence over the uplift is clear. Overall, the observed vertical rates oscillate between 0 and 3 mm/yr. Vertical motion can be more difficult to explain, as it is not necessarily related to tectonic processes and should be studied individually for each station. Several processes can be causing the subsidence, such as erosion and gravitational effects, that would affect each station differently.

In the eastern region of the Betics we identify subsidence related to the ground water extraction, which can result in the compaction of the soil, leading to vertical motion, (station ALHA). Also in this region, we observe an interesting behaviour, where a group of stations around the Carboneras and Alhama de Murcia faults move in the oppositive vertical sense, revealing dip-slip motion.

It is important to point out that vertical velocity's accuracy is not on par with the horizontal field. Some stations are measured to have higher than normal vertical motion. These anomalies can be understood by anthropogenic sources or unstable monuments or insufficient observation time.

In the Fig. 6, we have excluded vertical deformation with speeds higher than 5 mm/yr, as the measurements are assumed not realistic and/or anthropogenic and would affect to the clarity of the results.

V. CONCLUSIONS

From GPS techniques, we have obtained a three-dimensional crustal deformation velocity map coherent with previous results and tectonic plate theory. The results can serve as a baseline for future research on active geodynamics of the peninsula and have important implications for seismic hazard assessment.

Acknowledgments

First, I would like to thank my advisor Gia Khazaradze, which has been a great inspiration and has helped me tremendously during the making of this work. I also want to thank my family and friends for all the support and useful remarks.

[1] M. Palano, P. J. González, and J. Fernández, "The Diffuse Plate boundary of Nubia and Iberia in the Western Mediterranean: Crustal deformation evidence for viscous coupling and fragmented lithosphere," Earth and Planetary Science Letters, vol. 430, pp. 439–447, 2015, doi: 10.1016/j.epsl.2015.08.040.

[2] Y. Bock and S. Wdowinski, "GNSS Geodesy in Geophysics, Natural Hazards, Climate, and the Environment," in Position, Navigation, and Timing Technologies in the 21st Century: Integrated Satellite Navigation, Sensor Systems, and Civil Applications, vol. 1, Y. T. Jade Morton, Frank van Diggelen, James J. Spilker Jr., Bradford W. Parkinson, Sherman Lo, and Grace Gao, Eds. Wiley Online Library, 2021, pp. 741–820. doi: 10.1002/9781119458449.ch28.

[3] D. F. Argus, R. G. Gordon, and C. DeMets, "Geologically current motion of 56 plates relative to the no-net-rotation reference frame," Geochemistry Geophysics Geosystems, vol. 12, no. 11, p. Q11001, 2011, doi: 10.1029/2011GC003751.

[4] B. Andeweg, "Cenozoic tectonic evolution of the Iberian Peninsula: effects and causes of changing stress fields," Vrije Universiteit Amsterdam, 2002. [Online]. Available: http://www.falw.vu/~andb/iberia/thesispdf

[5] H. Perea, "The Catalan seismic crisis (1427 and 1428; NE Iberian Peninsula): Geological sources and earthquake triggering," Journal of Geodynamics, vol. 47, no. 5, pp. 259–270, May 2009, doi: 10.1016/j.jog.2009.01.002.

[6] D. Stich et al., "Seismicity of the Iberian Peninsula," in The Geology of Iberia: A Geodynamic Approach: Volume 5: Active Processes: Seismicity, Active Faulting and Relief, C. Quesada and J. T. Oliveira, Eds. Cham: Springer International Publishing, 2020, pp. 11–32. doi: 10.1007/978-3-030-10931-8_3.

[7] P. Bird, "An updated digital model of plate boundaries," Geochemistry, Geophysics, Geosystems, vol. 4, no. 3, 2003, doi: 10.1029/2001GC000252.

[8] "IGME (2015). QAFI v.3: Quaternary Faults Database of Iberia," 2015. http://info.igme.es/QAFI (accessed Apr. 20, 2022).

[9] P. Segall and J. L. Davis, "GPS applications for geodynamics and earthquake studies," Annual Review of Earth and Planetary Sciences, vol. 25, no. 1, pp. 301–336, 1997, doi: 10.1146/annurev.earth.25.1.301.

[10] T. Herring, R. W. King, and S. McClusky, "Introduction to GAMIT/GLOBK," Cambridge, MA, USA, 2010.

[11] Z. Altamimi, P. Rebischung, L. Métivier, and X. Collilieux, "ITRF2014: A new release of the International Terrestrial Reference Frame modeling nonlinear station motions," Journal of Geophysical Research: Solid Earth, vol. 121, no. 8, pp. 6109–6131, Aug. 2016, doi: 10.1002/2016JB013098.

[12] A. Echeverria, G. Khazaradze, E. Asensio, J. Gárate, J. Dávila-Martín, and E. Suriñach, "Crustal deformation in eastern Betics from CuaTeNeo GPS network," Tectonophysics, vol. 608, pp. 600–612, 2013, doi: 10.1016/j.tecto.2013.08.020.

[13] M. A. Floyd and T. A. Herring, "Fast Statistical Approaches to Geodetic Time Series Analysis," 2020, pp. 157–183. doi: 10.1007/978-3-030-21718-1_5.

[14] T. A. Herring, M. A. Floyd, M. Perry, and H. Soluxe, "Time series and error analysis GPS Data Processing and Analysis with GAMIT/GLOBK and track at ANU)." Accessed: Jun. 09, 2022. [Online]. Available: http://geoweb.mit.edu/~floyd/courses/gg/201807_Bishkek/